

12. PLEISTOCENE AND PLIOCENE TURBIDITES FROM THE IBERIA ABYSSAL PLAIN¹

D. Milkert,² P.P.E. Weaver,³ and L. Liu⁴

ABSTRACT

During Leg 149 a transect of holes (Sites 897 to 901) was drilled across the rifted continental margin off the west coast of Portugal at the edge of the Iberia Abyssal Plain. The upper part of the sedimentary sequence revealed the history of turbidite sedimentation on the plain. The sequence consists of thin terrigenous turbidites (0.1 to 1.0 m thick) separated by pelagic clay, marl, and ooze layers (0.01 to 1.89 m thick). Most of the turbidites consist of ungraded massive silts and clays, with sporadic coarser bases. Major input of terrigenous turbidites on the Iberia Abyssal Plain began in the late Pliocene at 2.6 Ma, but at Site 898 the lower part of the turbidite sequence is missing because of a hiatus. A large number of turbidites was deposited in the last 2.6 m.y., at an average of one turbidite per 3200 years at Hole 898A. It appears that sedimentation in the Iberian Basin is controlled at least partially by climatic changes.

INTRODUCTION

The Iberia Abyssal Plain lies west of the northern half of the Iberian Peninsula, west-southwest of Galicia Bank. It has an average water depth of 5300 m. The Iberia Abyssal Plain is connected to the north via Theta Gap to the Bay of Biscay, which is slightly shallower (4900 m). The total area of the plain is about 107,000 km² (Weaver et al., 1987), although to the west it passes into a series of deeper basins surrounded by hilly topography that have not been included in the area calculation. To the south, separating the Iberia Abyssal Plain from the Tagus Abyssal Plain, is an east-west-trending ridge incorporating the Tore Seamount (Fig. 1). Gorringer Bank builds the southern boundary to the Tagus Abyssal Plain and marks the surface expression of the active Eurasia/Africa plate boundary. To the east, the adjacent Iberia Margin has a straight narrow shelf and a steep continental slope. South of 40°N, the slope is cut by several large canyons. To the northwest of the Iberia Abyssal Plain area are a number of seamounts (Vigo, Vasco da Gama, and Porto), as well as the larger Galicia Bank.

With the exception of Ocean Drilling Program (ODP) Leg 103 (Boillot, Winterer, Meyer, et al., 1987; Comas and Maldonado, 1988), the sediments on the Iberia Abyssal Plain have not been studied in detail. Twenty-four cores from the plain were described by Davies (1967). They show thin micaceous sands with sharp bases, overlain by various colored muds and clays. Davies cautiously ascribed these sediments to turbidites and pelagic units, but provided no stratigraphy.

The principal objective of ODP Leg 149 was to determine the changes in the petrologic and physical nature of the acoustic basement across the ocean/continent transition. A secondary objective was to discover the history of late Cenozoic turbidite sedimentation, to date the deformation of sediments, and to compare this with the Miocene phase of compressional deformation in the Rif-Betic mountains of southern Spain and northern Africa.

Five sites (Sites 897 to 901) (Sawyer, Whitmarsh, Klaus, et al., 1994) were drilled along a 65-nmi west-east profile in water depths between 5320 m (Site 897) and 4730 m (Site 901) (Fig. 1). The drill sites differ by 284 m in water depth between the westernmost Site 897 and Site 900, and by 30 m between Holes 897A and 898A. Site 899 was drilled to 81.5 m below seafloor (mbsf), but only the lower part of the sequence was revealed. Site 901 was drilled to 182.0 mbsf, but Pleistocene and Pliocene turbidites are not a significant proportion of the recovery. Our investigation focuses on Sites 897, 898, and 900. The average recovery in lithologic Subunit IA (Pleistocene/Pliocene turbidites and pelagic material) reached 32.3% at Site 897, 99.9% at Site 898, and 62.1% at Site 900.

In this study we examine the sedimentology of the Pleistocene and Pliocene turbidite sequence, discuss the frequency of turbidity flows into the Iberia Abyssal Plain, and determine the timing of initiation of turbidity-current sedimentation.

GEOLOGICAL SETTING

The Leg 149 drill sites (Sites 897 to 901) were located over basement highs as required by the principle objective of the leg. However, the upper stratified turbidite sequence was recovered at Sites 897, 898, and 900, but not at Sites 899 and 901. Combined recovery from all sites comprises about 2400 m of Pleistocene to Upper Jurassic sediments. Figure 2 gives a composite interpreted seismic and sedimentary section through the Leg 149 sites (Sawyer, Whitmarsh, Klaus, et al., 1994). Vertical arrows adjacent to the summary columns indicate the thickness of sedimentary Unit IA, which comprises Pleistocene and Pliocene turbidite sequences and pelagic sediments.

The Pleistocene and upper Pliocene sedimentary sequence consists mainly of 0.1- to 1.0-m-thick turbidite units separated by thin pelagic layers (0.01 to 1.89 m thick) of clay, marl, and ooze. Sites 897 and 898 also contain thin layers of debris flows or slump structures. Beneath the Pliocene/Pleistocene sequence, a significant depositional hiatus extending back to the middle Miocene was found at Sites 897 and 898 (Sawyer, Whitmarsh, Klaus, et al., 1994). It is correlatable with a regional angular unconformity on seismic reflection profiles and may be related to northwest-southeast compression on this margin during a compressional phase in the Betic Mountains in southern Spain (Masson et al., 1994). This unit is underlain by Miocene to Oligocene terrigenous turbidites and pelagic sediments reworked by contour currents.

¹Whitmarsh, R.B., Sawyer, D.S., Klaus, A., and Masson, D.G. (Eds.), 1996. *Proc. ODP, Sci. Results*, 149: College Station, TX (Ocean Drilling Program).

²Geologisch-Paläontologisches Institut, Olshausenstr. 40, 24118 Kiel, Federal Republic of Germany. (Present address: Institute of Oceanographic Sciences Deacon Laboratory, Wormley, Godalming, Surrey GU8 5UB, United Kingdom.)
ngl29@rz.uni-kiel.d400.de

³Institute of Oceanographic Sciences Deacon Laboratory, Wormley, United Kingdom.

⁴Geology Department, Florida State University, Tallahassee, FL 32310, U.S.A.

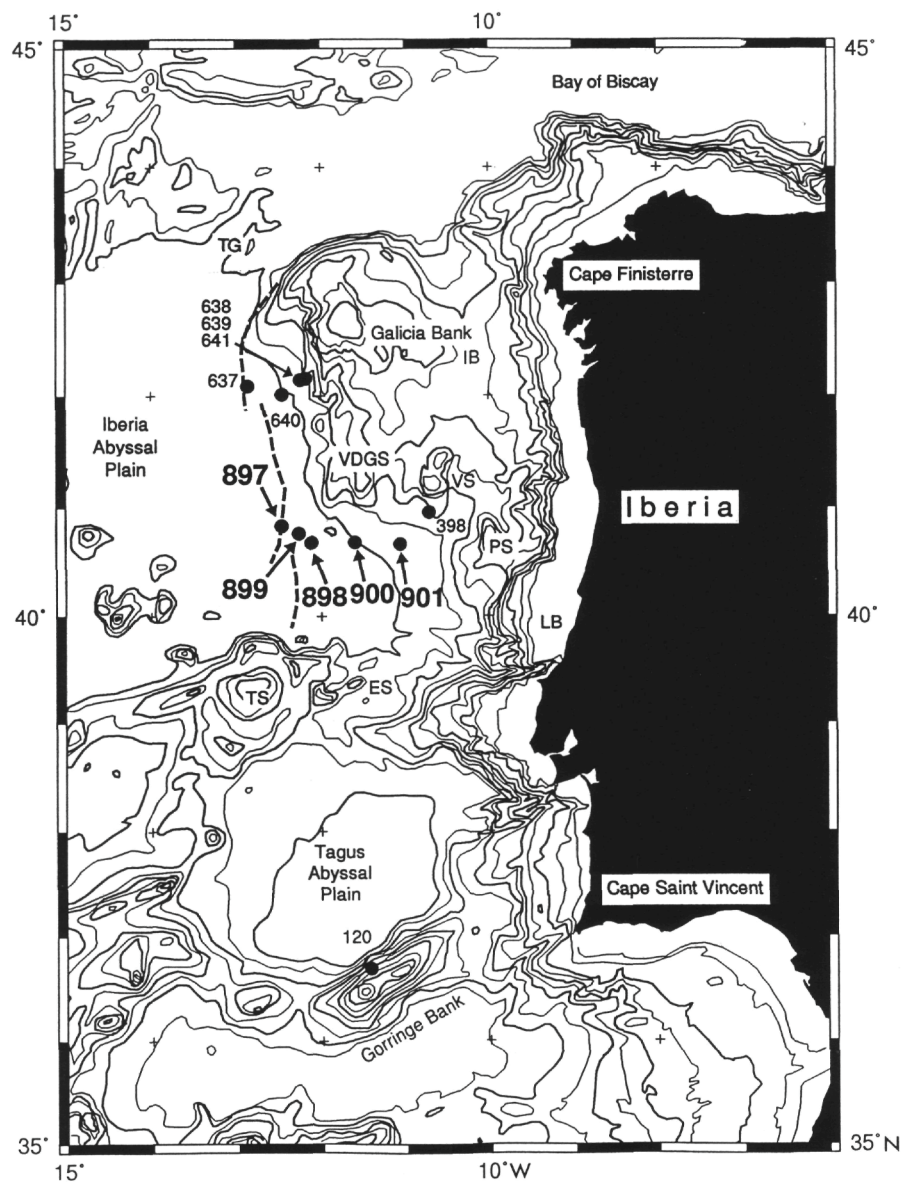


Figure 1. Bathymetry of the western Iberia Margin showing the location of Leg 149 Sites 897 to 901. The bold dashed line is the predicted location of the peridotite ridge (Beslier et al., 1993). Labels are: TG = Theta Gap; IB = Galicia Interior Basin; VDGS = Vasco da Gama Seamount; VS = Vigo Seamount; PS = Porto Seamount; LB = Lusitanian Basin; ES = Estremadura Spur; TS = Tore Seamount (modified from Sawyer, Whitmarsh, Klaus, et al., 1994).

METHODS

Samples were taken from selected intervals of the Pleistocene and Pliocene sediment sequence at Sites 897, 898, and 900. The sampling interval was varied according to the thickness and variations of individual beds. In general, complete turbidite sequences and most of the pelagic sediments were sampled (in total, 417 samples). Individual samples were analyzed to determine their calcium carbonate (CaCO_3) and organic carbon contents, grain-size characteristics, and major, minor, and trace-element distribution.

Samples for geochemical analysis were oven-dried at 110°C and mechanically ground in agate. Calcium carbonate was determined using Coulometric detection of the carbon dioxide evolved during acid attack of 25-mg samples. Precision, measured by replicate analyses, was better than 1%-2%. Total carbon was determined using Coulometric detection of carbon dioxide evolved on combustion of samples burned at 900°C . Organic carbon was then determined by the differ-

ence. Major, minor, and trace-element analyses were performed by inductively coupled plasma atomic emission spectroscopy (ICP-AES) after digestion of samples with a combination of hydrofluoric, perchloride, and nitric acids (Totland et al., 1992). Accuracy was checked using standard reference materials. Precision was 3%-5% for all elements (Al, Fe, Mn, Mg, Li, Mo, Ni, Pb, Sc, Sr, V, Y, Na, K, Ti, P, Ba, Co, Cr, Cu, Zn, and Zr).

Grain-size characteristics were determined by using a Sedigraph 5000 ET particle analyzer. About 4 cm^3 of sample was used for each grain-size analysis. Each sediment sample was prepared by adding distilled water containing 0.5% sodium hexametaphosphate, used as an antiflocculant. Samples were disaggregated for 24 hr and diluted further and analyzed. The Sedigraph 5000 ET produces acceptably accurate measurements only for sediments of a grain size smaller than $70\ \mu\text{m}$. Coarser sand samples were sieved at $63\ \mu\text{m}$ prior to the sedigraph measurements. Percentages of sand and silt, silt/clay ratio, and median grain size (Md 50) were determined from the resulting

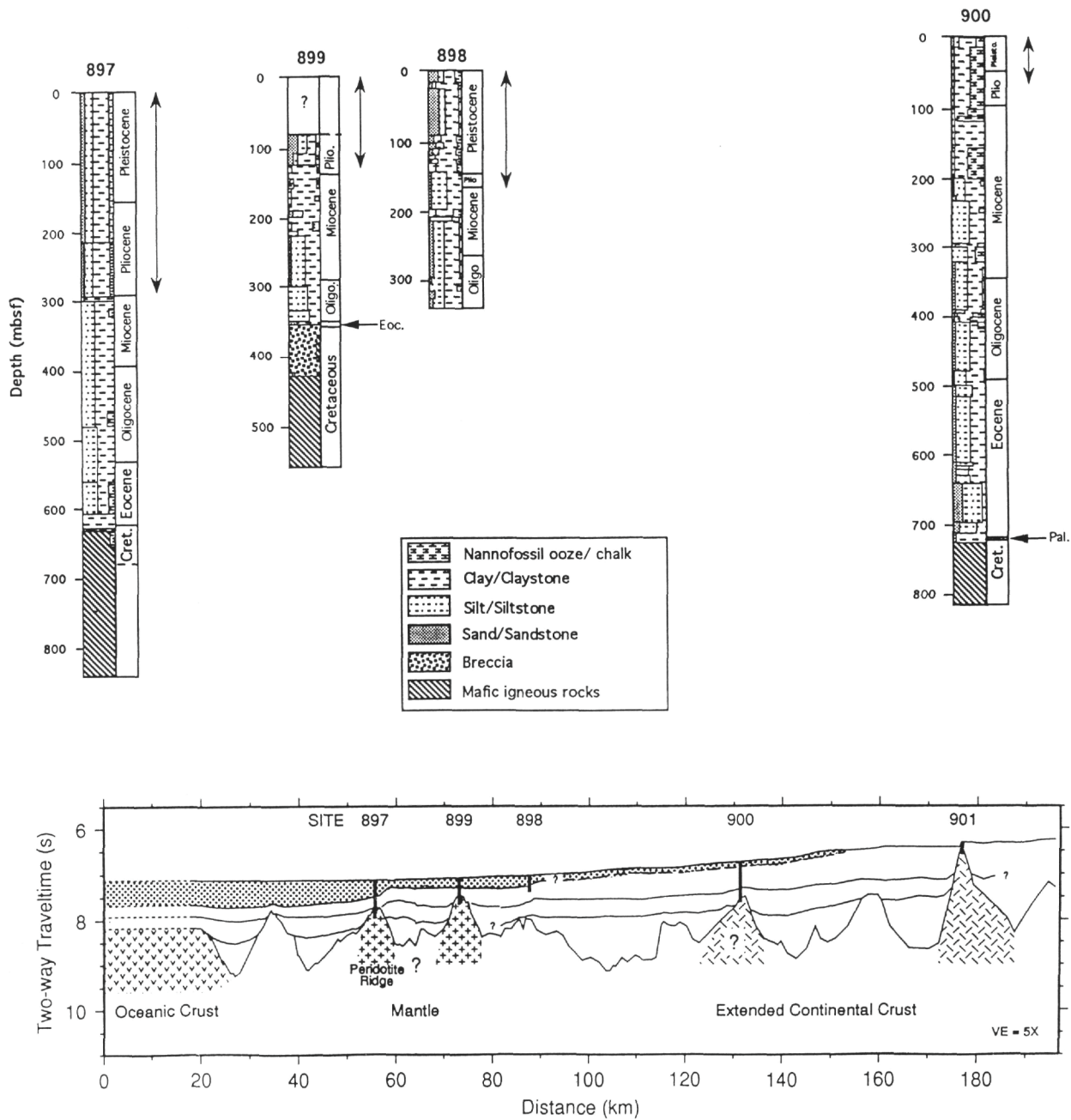


Figure 2. Summary of lithologic columns for Sites 897 to 900 and a composite interpreted seismic section through these sites (see Fig. 1). Vertical arrows indicate the distribution of Pleistocene and Pliocene terrigenous turbidites and pelagic sediments (Subunit IA) in the lithologic column (modified from Sawyer, Whitmarsh, Klaus, et al., 1994). Shading in the seismic section indicates the same unit.

granulometric curves. The percentage of material within each 0.25-phi size class was calculated and plotted as a frequency distribution curve with arithmetic ordinates (grain-size spectra; Wentworth, 1922). Variable sorting values are defined as the inclusive graphic standard deviation of Folk (1974). These were then stacked on top of one another to identify persistent modes and modal variations throughout the turbidites.

RESULTS

Sediment Lithologies and Characteristics

Pleistocene and Pliocene sediments on the Iberia Abyssal Plain consist of pelagic sediments and turbidites. Percentages of turbidite

vs. pelagic sediments at Sites 897, 898, and 900 are shown on Figure 3. At Holes 897C and 898A, parts of debris-flow deposits were also observed (Cores 149-897C-22R and 149-898A-12H).

Pelagic Sediments

The pelagic sediments consist of clays, marls, and oozes. At this water depth the proportion of calcium carbonate varies cyclically (Fig. 4A), in relation to bottom-water variations, a well-known phenomenon in many North Atlantic basins (Weaver and Kuijpers, 1983; Raymo et al., 1987). At present and during other Pliocene/Pleistocene interglacials, the area lies within the lysocline, but above the carbonate compensation depth (CCD) and thus carbonate can accumulate on the seafloor. During glacial intervals the influence of cor-

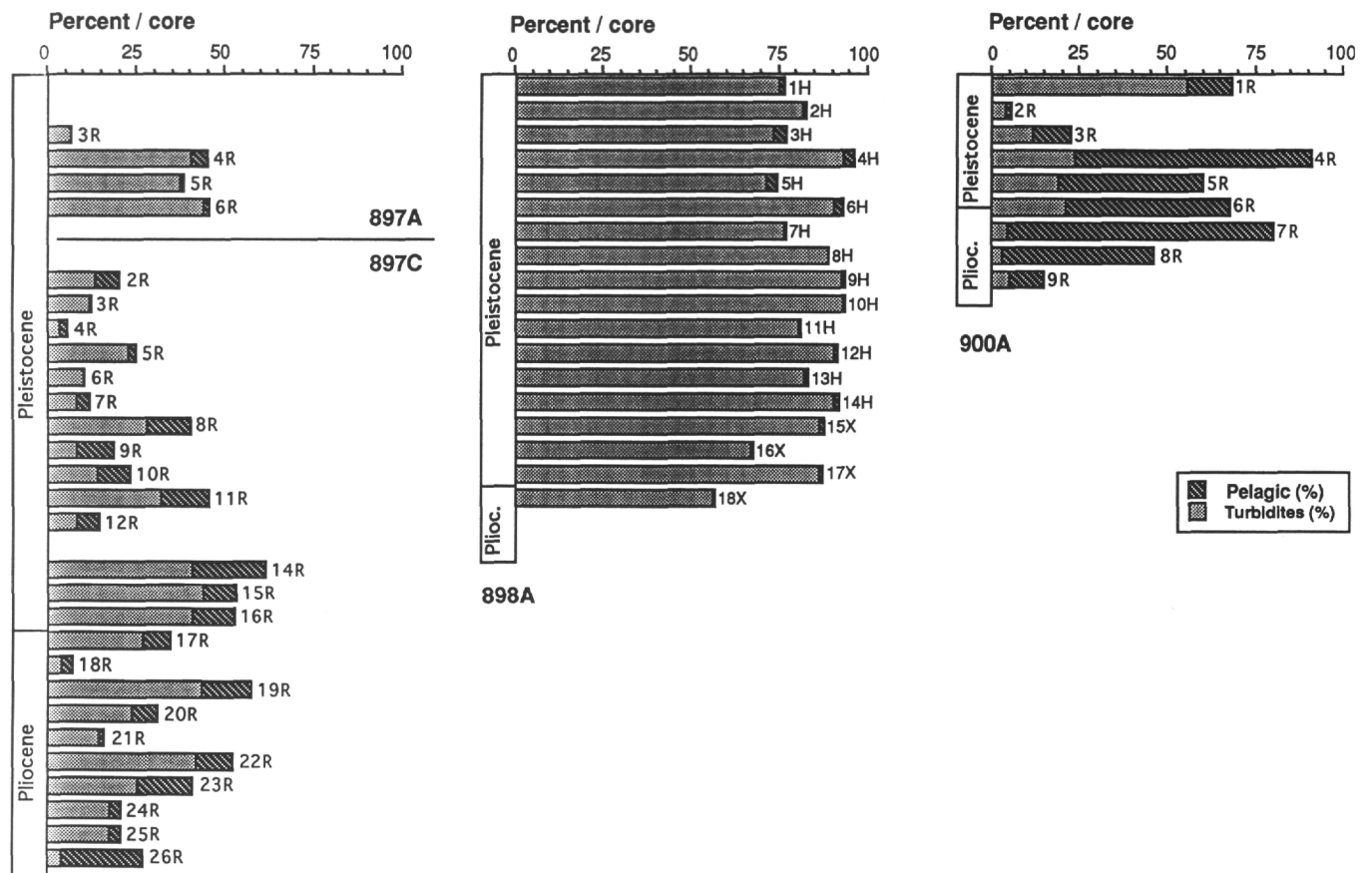


Figure 3. Percentage of turbidite vs. pelagic sediments in lithologic Subunit IA at Sites 897, 898, and 900. The total percentage for any core is estimated to the percentage recovery in that core.

rosive Antarctic Bottom Water leads to increased dissolution (Berger, 1968; Crowley, 1983; Weaver and Kuijpers, 1983) and subsequent deposition of pelagic clays.

Pelagic layers vary in thickness between 0.01 and 1.89 m. The variation in thickness occurs in all sites, with the thickest pelagic layers observed at Site 900. Table 1 shows total, average, and maximum thicknesses of pelagic lithologies at Sites 897, 898, and 900.

Color

The pelagic sediments vary in color from white (N9) to greenish gray (5GY 5/1) at Site 897, from medium gray (N5) to dark yellowish brown (10YR 4/2) at Site 898, and from white (N2,3) through yellowish gray (5Y 8/1) to greenish gray (5GY 6/1) at Site 900 (after description by shipboard scientists, Sawyer, Whitmarsh, Klaus, et al., 1994).

Carbonate Content and Organic Carbon

The pelagic sediments contain an average 45% CaCO₃ and an average 0.31% organic carbon. The values for each site are shown in Table 1. Figure 4A shows the cyclical variations of CaCO₃ in pelagic sediments at Site 898 within the Pliocene/Pleistocene. Figure 4B shows the generally low values of organic carbon in the pelagic sediments.

Bioturbation

The pelagic sediments show slight to moderate mottling caused by bioturbation, but no distinct ichnofauna is visible. Bioturbation continues downward from the pelagic sediments into the top of the underlying turbidites.

Turbidite Characteristics

Pleistocene and Pliocene sedimentation at Sites 897, 898, and 900 was dominated by the deposition of terrigenous turbidites, separated by thin pelagic layers (see the data tables on the CD-ROM in back pocket of *Initial Reports* Volume 157). Turbidite sequences are easily distinguished from pelagic sediments by their graded bases, distinctive darker colors, and, usually, lack of bioturbation. When fresh they were olive gray (5Y 4/1) or dark olive gray (5Y 2/1), but they rapidly oxidized to light olive gray (5Y 6/1) or olive gray (5Y 4/1). The base of each turbidite is clearly defined as a sharp boundary over mottled, lighter-colored pelagic sediment. The structureless to laminated basal sand and silt layers in the turbidites correspond to the Tc-d division of Bouma (1962); the Ta-b interval is absent. Clay-rich intervals are bioturbated to laminated, contain significant amounts of reworked nannofossils, and correspond to the turbidite mud divisions (Tel-3) of Stow and Piper (1984). Visually distinguishing the Te facies from the pelagic interval is difficult in areas where fine-grained pelagic sediments are mixed downward by bioturbation and drilling disturbance. The boundary is generally taken at the point where both pelagic and turbidite sediments are represented equally. Sedimentary structures are developed at the base of the turbidites. In many cases silty lamination is visible to the eye. Several examples show a finely laminated silty mud overlain by a distinct, 1- to 20-cm-thick layer including single 0.3- to 0.5-cm-thick silt layers; this part of the sequence is capped by uniform mud (Te division) (e.g., Section 149-898A-5H-4, 127-132 cm; see also Section 5H-6, 65-126 cm; Sawyer, Whitmarsh, Klaus, et al., 1994).

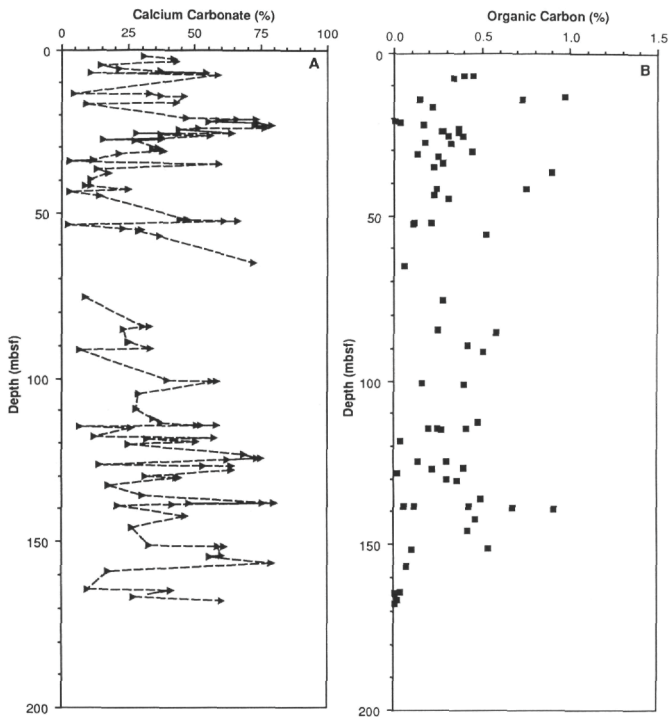


Figure 4. Distribution of CaCO₃ and organic carbon in pelagic sediments at Site 898. The CaCO₃ content shows cyclic variations related to climatic changes. The organic carbon shows the generally low values in pelagic sediments.

The terrigenous turbidites appeared very similar throughout the sedimentary sequence during shipboard description. More detailed post-cruise examination and additional visual core descriptions allowed a separation of these turbidites into four groups on the basis of different color and lithologic composition. Figure 5 shows the distribution of these types with core depth at Hole 898A.

1. Gray terrigenous/siliceous turbidites are usually olive gray (5Y 4/1) to greenish black (5G 2/1) in color, with CaCO₃ contents between 3% to 22% and high organic carbon contents (between 0.3% and 2.5%) (Fig. 6). The bases are coarse sand to silt and commonly mica rich. Green turbidites dominate the Pliocene and Pleistocene sequence (Fig. 5).
2. Mixed gray/calcareous, terrigenous turbidites with sandy, silty bases are less common. The carbonate content increases in relation to gray turbidites (Fig. 6). The color varies from light olive gray (5Y 6/1) to olive gray (5Y 4/1).
3. Calcareous turbidites (light olive gray, 5Y 6/1, to medium gray, N5) consist of coccolith mud over foraminiferal sand at the base and have a CaCO₃ content of 17% to 53% in the turbidite mud (Fig. 6).
4. Brownish-reddish sandy turbidites are common at all sites in the lower Pleistocene. The Te division is olive gray (5Y 4/1) to medium dark gray (N4) and commonly overlies a laminated, brownish Td division. This turbidite group generally has low CaCO₃ contents (10% to 15%) and higher organic carbon (0.4% to >1%) (Fig. 6) compared with the other types of turbidites.

All turbidite types show silty lamination in the Te division. The frequency of turbidites with coarser, laminated bases increases after Zone NN19h (1.95 to 2.44 m.y.; Shackleton et al., 1995). Despite the visual differences, geochemical and sedimentological analyses do

Table 1. Characteristics of pelagic sediments at Sites 897, 898, and 900.

	897	898	900
Water depth (mbsf)	5315	5279	5037
Total thickness of Subunit IA (m)	292.0	163.4	67.2
Total thickness of pelagic sediments (m)	19.83	23.96	67.2
Average thickness of single layer (m)	0.06	0.06	0.49
Minimum thickness of single layer (m)	0.01	0.002	0.03
Maximum thickness of single layer (m)	0.98	0.39	1.89
Average CaCO ₃ (%)	28.99	45.89	61.18
Minimum CaCO ₃ (%)	2.0	8.86	3.10
Maximum CaCO ₃ (%)	77.30	80.0	73.10
Average organic carbon (%)	0.39	0.31	0.25
Minimum organic carbon (%)	0.04	0.01	0.08
Maximum organic carbon (%)	1.21	0.91	0.48

not show distinct compositional groups of turbidites but rather a gradation from one type to another.

A huge number of turbidites was deposited in the last 2 m.y., as shown in Table 2. A maximum occurrence of 48 turbidites (4 to 60 cm thick) was recognized in a single 9.5-m core (Core 149-898 A-14H). In general the frequency of the turbidites varies from 2 to 7 per meter throughout the cores. The large number of single turbidites (e.g., 600 in Hole 898A, Table 2) makes it impossible to correlate individual units between the sites.

Owing to the poor recovery at Sites 897 and 900, investigation focused mainly on Site 898, and most of the carbonate and geochemical profiles were determined at this location to verify the different types of turbidites and sedimentation patterns through the Pleistocene and Pliocene.

Color

Turbidite sequence colors are similar at all sites (897 to 900). The turbidite base (Td division sand or silt) shows generally dark colors (dark yellowish brown, 10YR 4/2; dark greenish gray, 5GY 4/1; olive black, 5Y 2/1; or olive gray, 5Y 4/1). The turbidite mud sequences (Te division) show colors similar to the Td unit, with additional brownish gray (5YR 4/1) and greenish gray (5GY 6/1) to light greenish gray (5G Y 8/1) clays.

Calcium Carbonate and Organic Carbon

Overall, there are no major differences in the CaCO₃ content of the turbidite muds (Te division) or turbidite sands (Td division) at the different drill sites (Table 2). The CaCO₃ content of the turbidite sequences shows an average of about 20% for both the Td and Te divisions. CaCO₃ values for the turbidite sands (Table 2) vary from a minimum of 3.76% to a maximum of 72.69% at Hole 898A. Turbidite muds show similar differences, with a maximum of 78.10% and a minimum of 0.84% at Hole 897C. Figure 6 displays the variations in calcium carbonate content within the various types of turbidites at Site 898 for both turbidite sands (Td division) and turbidite muds (Te division).

The organic carbon content shows the highest values at Site 897, with an average of 0.6% for both the Td and Te divisions (Table 2), and declines toward the continental margin at Site 900 to 0.02% for the Td division and 0.3% for the Te turbidite mud. Figure 6 exhibits the variations in organic carbon content in the turbidite sands (Td division) and turbidite muds (Te division) at Site 898.

Bioturbation

The turbidite muds are homogeneous and show no obvious effects of bioturbation except in the upper few centimeters, which are typically bioturbated from the overlying pelagic layers.

Grain-size Characteristics

A summary of the grain-size analyses for Hole 898A is given in Table 3. Td division sediment contains more than 30% sand-sized material (>63 μm) (Fig. 7). The median grain size, sorting, and skew-

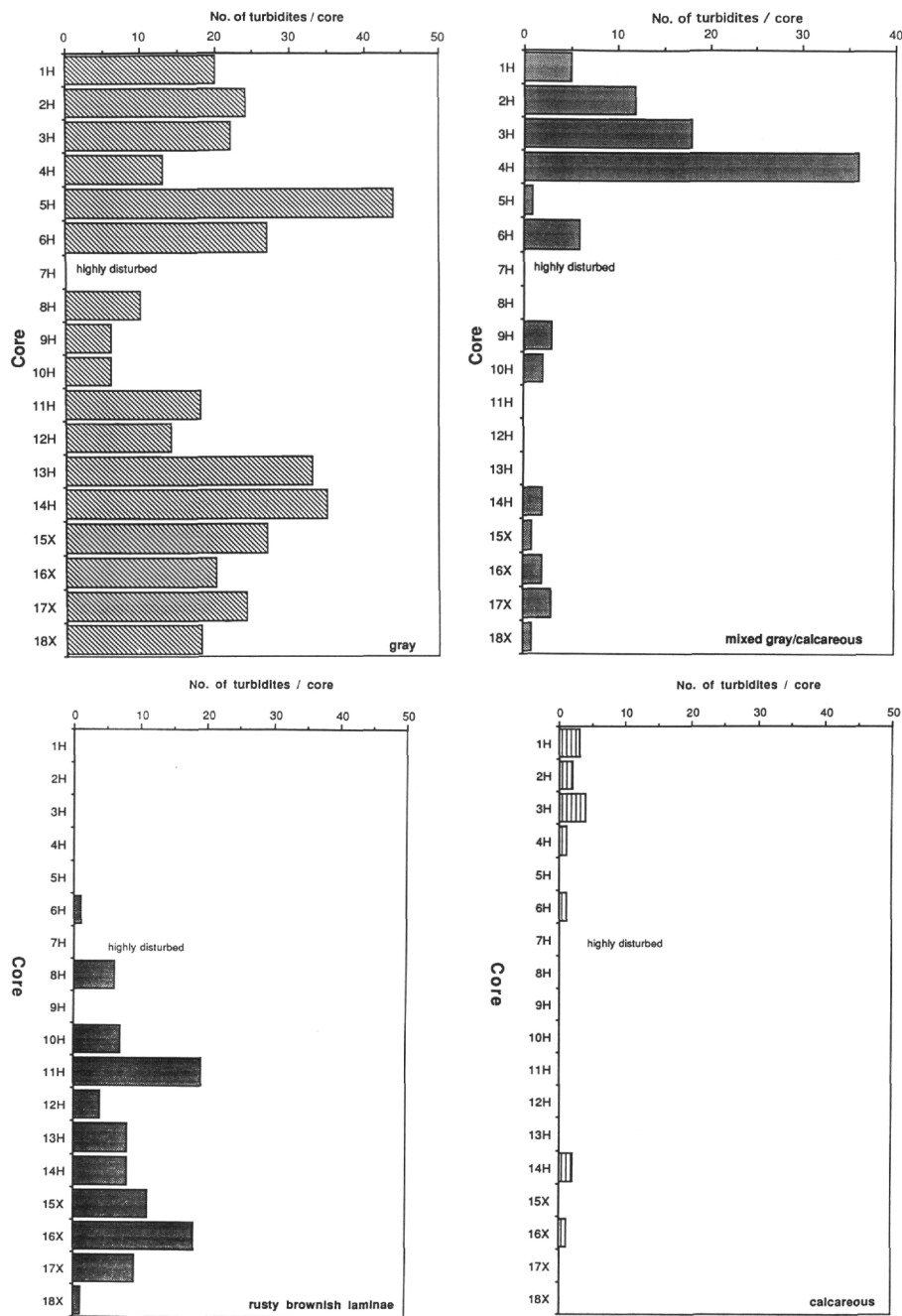


Figure 5. Distribution of four types of turbidites in Hole 898A based on visual descriptions.

ness for turbidite sands at Site 898 in Figure 8 are highly variable throughout the sequence with generally poor sorting. The average grain-size parameters for turbidite muds (Te division) show more than 50% silt-grade material and usually less than 1 % sand-sized material (Table 3). The content of sand and silt reflects the presence and distribution of terrigenous sand material and foraminifers (Fig. 7). The turbidite muds are ungraded and largely compose the Te3 structural division of Stow and Piper (1984).

Geochemical Characteristics

ICP-AES analysis of major and minor elements in sediment samples from visually identified turbidites shows great similarities throughout the different types of turbidites. Plotting the distribution

of the turbidites in a triangular diagram (Fig. 9) with Al₂O₃, CaO, and MgO as end-members to give an estimate of the origin of the turbidites compared to the main composition of granites, basalts and peridotites (Matthes, 1983) shows that the turbidites originate mainly from continental erosion.

The extreme range of carbonate contents makes variation in the distribution of major elements (e.g., TiO₂, Al₂O₃, Fe₂O₃, MgO, Na₂O, and K₂O) difficult to assess. Therefore, all elements were recalculated to a carbonate-free basis. The average thickness of the Iberia Abyssal Plain turbidites indicates that they will have been almost completely affected by redox-controlled early diagenetic processes (Jarvis and Higgs, 1987). Al, Ti, Mg, and Zr appear to be unaffected by changing redox conditions (Jarvis et al., 1988; Pearce and Jarvis, in press).

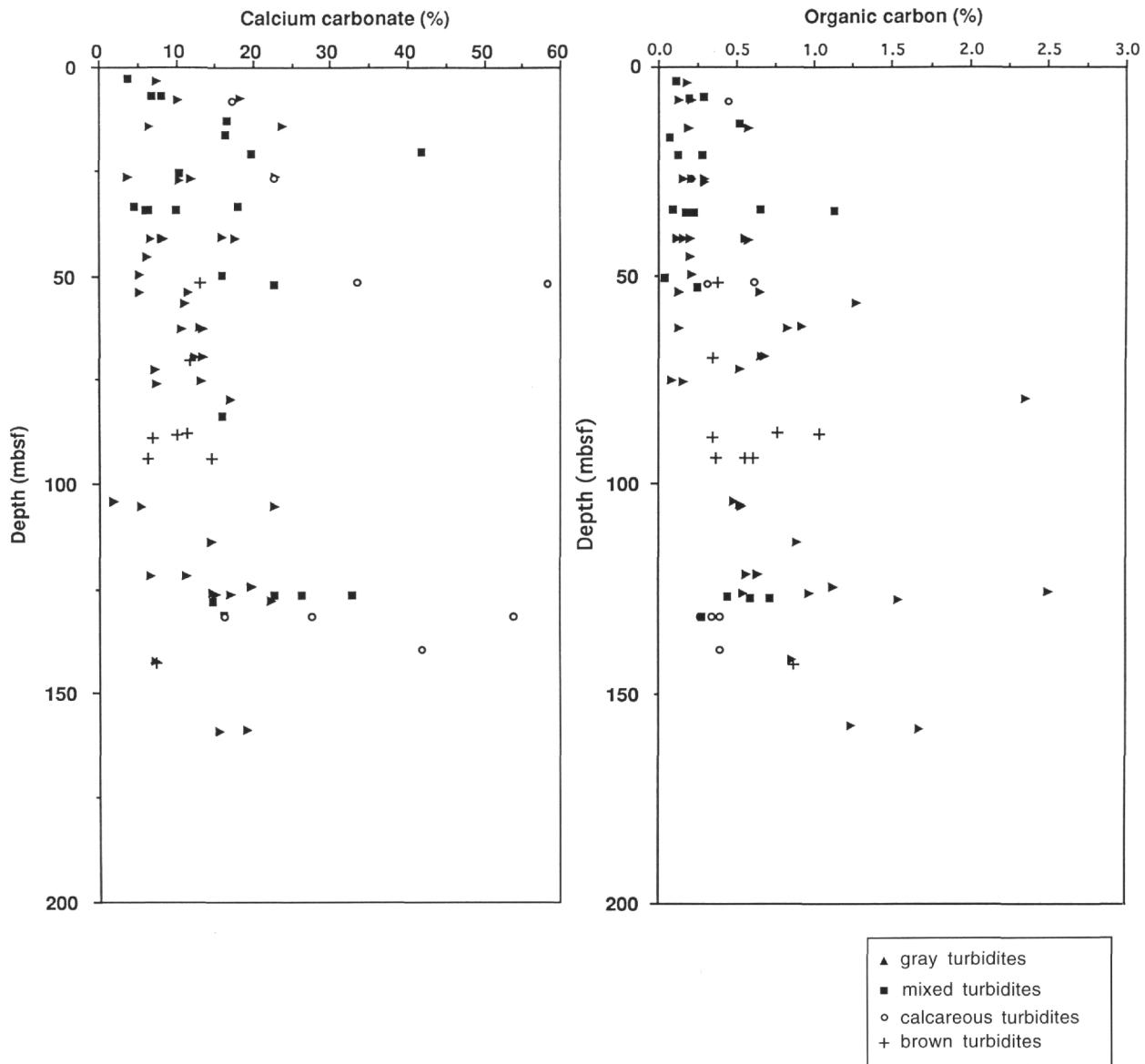


Figure 6. CaCO₃ and organic carbon contents in the Td and Te divisions at Hole 898A for the different types of turbidites.

In general, the Iberia Abyssal Plain turbidites have low Fe, Mg, Ti, and Zr contents with high proportions of Al and alkali metals. This indicates a continental provenance for the aluminosilicate phases and confirms a continental source region, similar to the element distribution described for organic-rich turbidites on the Madeira Abyssal Plain by de Lange et al. (1987). The Iberia Abyssal Plain data (Fig. 10), however, do not show the clustering recognized by de Lange et al. (1987), which is due to different sediment composition in the various source areas. These data probably indicate a constant composition of the continental-derived material, rather than a single source for the Iberia Abyssal Plain turbidites.

Slump and Slide Structures

Cores 149-897C-22R and 149-898A-12H contain sediments with disturbed sedimentary structures. Section 149-897C-22R-3 shows a 1.3-m-thick, highly folded and scrambled mixture of pelagic oozes and silty sands (Td division) with a small amount of turbidite clays. The sequence is early Pliocene in age (NN18 after Liu, this volume; N20/19 after Gervais, this volume). It is interpreted as a minor debris flow.

An inverted turbidite sequence was obtained from Section 149-898A-12H-1. The turbidite characteristics are similar to those of the other Site 898 cores. The inverted sequence is 83 cm thick and includes three turbidites, which are turned upside down. It is underlain by an unusual, more than 1-m-thick Te mud of homogeneous structure. This flow is of late Pleistocene age (NN19d after Liu, this volume; N23/22 after Gervais, this volume). This section is interpreted as a single block, which was turned over by a gravity flow.

The above-described structures are not correlatable between the drill sites, which indicates that they originated as different events that did not occur at the other locations.

PLEISTOCENE AND PLIOCENE DEPOSITIONAL HISTORY

The Pleistocene and Pliocene turbidites on the Iberia Abyssal Plain represent a distinct change in sediment type from the contourites, mud turbidites, and pelagic sediments beneath.

Table 2. Characteristics of turbidites at Sites 897, 898, and 900.

	897	898	900
Water depth (mbsf)	5315	5279	5037
Recovery (%)	41.2	94.3	62.2
Total thickness of Subunit IA (m)	292.0	163.4	67.2
Total number of turbidites	410	600	67
Total thickness of turbidites (m)	58.36	115.5	11.36
Average thickness of single turbidite (m)	0.15	0.19	0.15
Minimum thickness of single turbidite (m)	0.01	0.01	0.02
Maximum thickness of single turbidite (m)	1.73	1.93	0.35
Minimum thickness of Td (m)	0.001	0.02	0.002
Maximum thickness of Td (m)	0.86	1.88	0.21
Average CaCO ₃ (%) Td	22.04	13.85	23.25
Average CaCO ₃ (%) Te	23.87	17.27	18.97
Minimum CaCO ₃ (%) Td	3.81	3.76	5.70
Minimum CaCO ₃ (%) Te	0.84	1.47	1.75
Maximum CaCO ₃ (%) Td	65.30	72.69	28.60
Maximum CaCO ₃ (%) Te	78.10	55.00	49.10
Average organic carbon (%) Td	0.62	0.40	0.02
Average organic carbon (%) Te	0.66	0.63	0.33
Minimum organic carbon (%) Td	0.24	0.01	0.02
Minimum organic carbon (%) Te	0.07	0.01	0.04
Maximum organic carbon (%) Td	2.74	2.36	0.02
Maximum organic carbon (%) Te	1.75	3.33	0.53

Table 3. Grain-size characteristics at Hole 898A.

	Total	Gray	Mixed	Calcareous	Brown
Td division (turbidite sand)					
Average sand (%)	32.57	37.26	33.40	28.50	23.25
Average silt (%)	51.93	49.56	46.17	53.70	64.49
Average clay (%)	15.21	13.18	14.61	18.00	12.26
Md 50	18.24	18.25	17.40	16.85	24.80
Median	13.71	12.51	14.00	15.63	20.05
Sorting	13.86	13.24	14.57	13.22	16.89
Skewness	0.21	0.10	0.24	1.02	0.02
Te division (turbidite mud)					
Average sand (%)	0.26	0.11	2.17	0.00	0.00
Average silt (%)	52.90	53.83	49.88	55.33	46.67
Average clay (%)	46.84	46.06	47.95	44.70	53.33
Md 50	3.65	3.23	7.88	8.03	1.64
Median	5.48	5.69	7.20	6.72	3.95
Sorting	7.16	7.08	8.59	9.25	5.87
Skewness	0.66	0.68	0.50	0.45	0.78

Sites 897, 898, and 900 all show middle Miocene contourite sequences interbedded with pelagic clays (Comas, this volume). Parts of the middle Miocene to upper Pliocene are missing from Sites 897 and 898 because of a hiatus associated with crustal compression during the middle Miocene (Masson et al., 1994; Sawyer, Whitmarsh, Klaus, et al., 1994). The sediment sequence is more complete at Site 900, where the middle Miocene contourites pass upward into a sequence of thin mud turbidites interbedded with pelagic sediments at about 15.8 Ma (Fig. 11). The number of turbidites decreases gradually upward during the upper Miocene (N17, at about 9.9 to 8.2 Ma; Gervais, this volume) from Cores 149-900A-15R (123.9 mbsf) to 12R (98 mbsf). In mid-Zone NN11 (5.56-8.4 Ma; Shackleton et al., 1995) they disappear completely, giving way to a continuous sequence of pelagic marls. The marls continue to 67.2 mbsf (Core 149-900A-9R), where the Pliocene/Pleistocene turbidite sequence begins abruptly. The age of the onset of terrigenous turbidite deposition is 2.6 Ma, based on the nannofossil data.

The late Miocene hiatus at Site 897 occurs at the top of the contourite sequence and represents a sediment gap from NN4 (between 15.8 and 18.4 Ma; Shackleton et al., 1995) to 7.8 Ma (Fig. 11). Above the hiatus is 9.25 m of pelagic clays, succeeded by the Pliocene/Pleistocene turbidite sequence. The age of the base of these turbidites is 2.6 Ma, the same as at Site 900.

At Site 898 the hiatus extends from NN7 (between 10.7 and 12.2 Ma; Shackleton et al., 1995) to 2.0 Ma and has 8.82 m of pelagic clay overlying the contourites beneath it (Fig. 11). The Pliocene/Pleistocene turbidites begin immediately above the hiatus, and, therefore, the age of their onset here is slightly later than at Holes 897C and 900A.

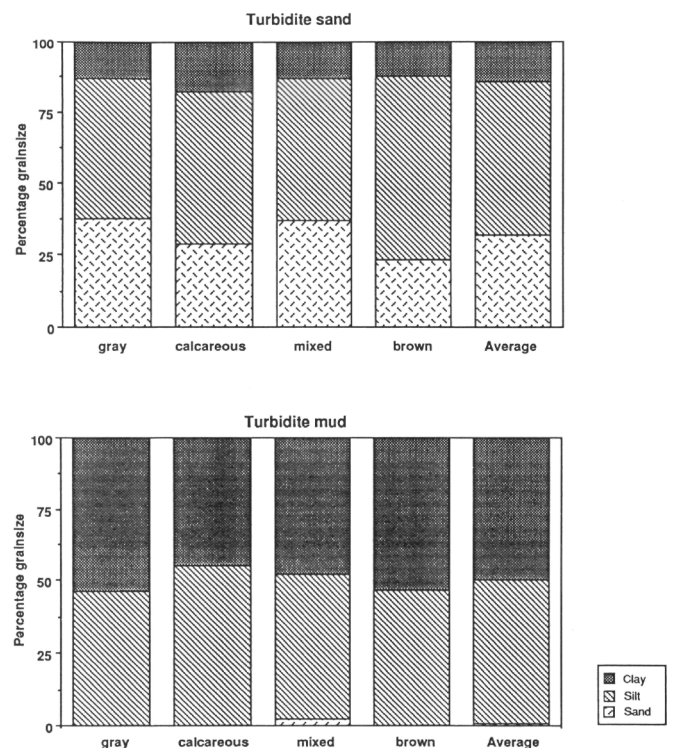


Figure 7. Percentage of grain sizes (sand/silt/clay ratio) in turbidite sand (Td division) and turbidite mud (Te division) in different types of turbidites at Hole 898A.

Thus, the inception of Pliocene/Pleistocene turbidite deposition appears to have been at 2.6 Ma and to have followed a period of quiet pelagic accumulation at both Holes 897C and 900A. At Hole 898A, however, the earliest turbidites may have been eroded away, giving an apparently later age. Following the initiation of turbidite sedimentation, the deposition of similar lithologies has continued up to the present day.

Accumulation rates for the Cenozoic sediments at Sites 897, 898, and 900 are shown in Figure 12. The accumulation rate of 13 m/m.y. calculated for Site 898 (Fig. 12) is consistent with accumulation within the lysocline but above the CCD, where a portion of the CaCO₃ deposited on the seabed is dissolved before burial. At Site 897, the pelagic clay sequence immediately beneath the Pliocene/Pleistocene

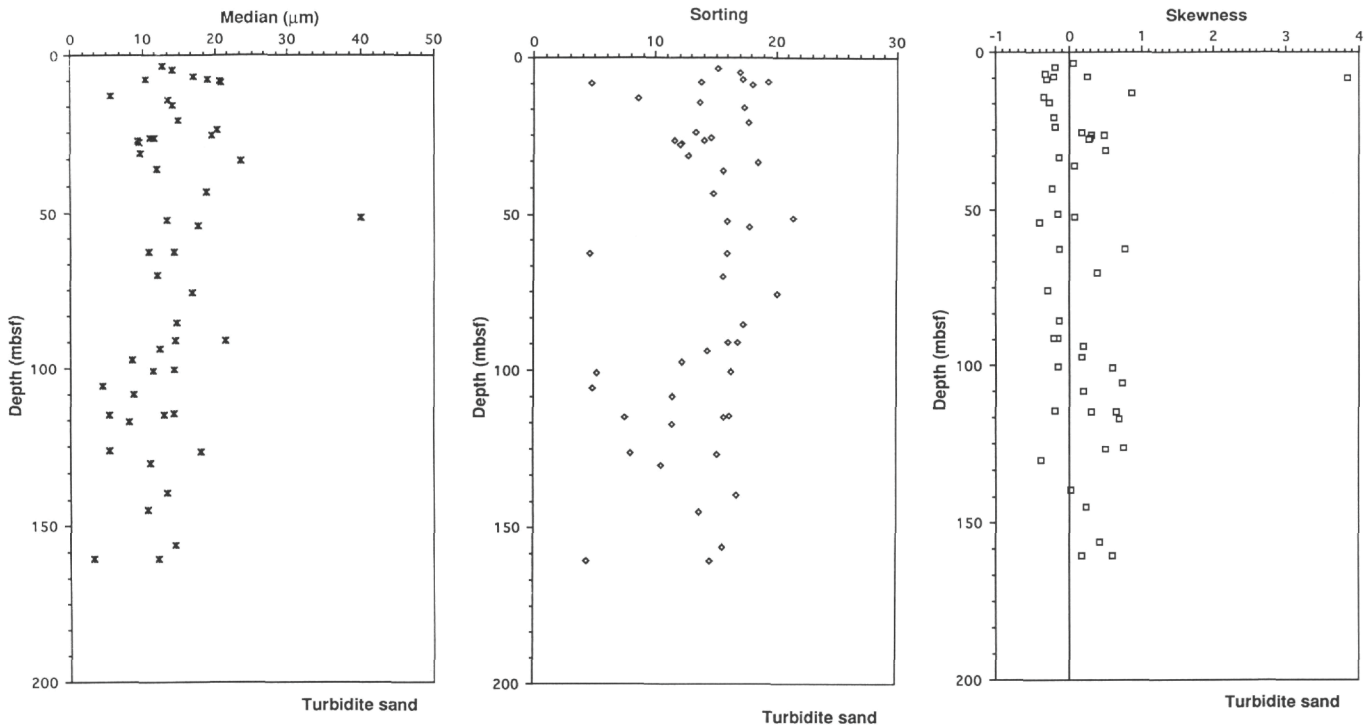


Figure 8. Grain-size characteristics at Hole 898A for the turbidite sand (Td division).

turbidites has an accumulation rate of 4.2 m/m.y. (Fig. 12). This is consistent with a raised CCD prior to the onset of Northern Hemisphere glaciation at 2.6 Ma. Prior to this time, the deep basins of the North Atlantic lay permanently below the CCD (Weaver et al., 1986). Such severe dissolution prior to 2.6 Ma does not seem to have affected Site 900, which lies at a water depth of 5036 m, only 284 m shallower than Site 897. At this site, marls with CaCO_3 contents of 20%-70% and an average accumulation rate of 10.6 m/m.y. were deposited between mid-Zone NN11 (5.56-8.4 Ma; Shackleton et al., 1995) and 2.6 Ma. This may indicate that the CCD lay between 5036 and 5320 m in this area during the early Pliocene.

The average accumulation rate over the whole Pliocene/Pleistocene turbidite sequence varies among the three sites, increasing with increasing water depth. At Site 897 it averages 98 m/m.y. (Fig. 13A). At Site 898 the overall average is 92 m/m.y., but rates vary from 64.8 m/m.y. between 1.95 and 1.46 Ma to a rapid 167 m/m.y. from 1.46 to 1 Ma and then back to 71 m/m.y. from 1 Ma to the present day (Fig. 13B). This interval of higher accumulation rate corresponds in part with thicker and more sandy turbidites, which occur in Cores 149-898A-8H to 10H. The sedimentation rate at Site 900 (25.8 m/m.y.) is fairly constant through the Pleistocene (Fig. 13C) and declines to 10.6 m/m.y. for the upper Pliocene.

The accumulation rates reveal only the total amount of sediment deposited with time and make no distinction between the volume of individual flows and their frequency. In Figure 14 we plotted the number of turbidites deposited per time unit. For Site 898, where there is nearly complete core recovery, 200-k.y. time slices were chosen, but, for Site 900, where recovery was less, we used 400-k.y. time slices and estimated the numbers of turbidites by grossing-upward for the missed intervals. Core recovery at Site 897 was too poor to complete the same exercise. The ages and depths were taken from the accumulation-rate plots in Figure 12. The results show considerable variation in the frequency of turbidity currents. For Site 898 these build up in frequency from 20.5 flows/100 k.y. between 1.8 and 2 Ma (which means 1 turbidite per 4900 yr) to 64 flows/100 k.y. between 1.2 to 1.4 Ma (which equals 1 turbidite per 1600 yr); the frequency then reduces gradually to the present day. The low frequency of flows

between 1 and 1.2 Ma (12.5 flows/100 k.y., 1 turbidite per 8000 yr) coincides with the interval of thick turbidite flows mentioned above. Because Site 898 is located on the abyssal plain, this frequency can be taken to represent the frequency of turbidite deposition for the whole plain.

Site 900 shows a much lower frequency of turbidite deposition with the highest rates (8 flows/100 k.y.) between 1.6 and 2 Ma. The lower frequency of flows deposited at Site 900 may be due to its higher elevation, 254 m above the level of Site 898. Presumably only the largest flows on the abyssal plain would reach up to this height above the plain, although others may be deposited by passing turbidity currents moving down the continental slope.

DISCUSSION

The coincidence of the 2.6 Ma age of onset of turbidite deposition with the onset of Northern Hemisphere glaciation (Shackleton et al., 1984) is striking. Weaver and Kuijpers (1983) showed a link between climate/sea-level change and turbidite deposition on the Madeira Abyssal Plain, and Weaver et al. (1986) postulated that the Madeira Abyssal Plain would receive turbidites during periods of climatic oscillation such as the 2.6 Ma to recent interval. The onset of turbidite deposition at 2.6 Ma suggests that sedimentation in the Iberian Basin is controlled at least partially by climatic change. However, the frequency of turbidite input is much greater than in the Madeira Abyssal Plain and individual turbidites are clearly not related to particular sea-level changes, as they are for the Madeira Abyssal Plain. It may be that the lowering of sea level, associated with the buildup of Northern Hemisphere ice, caused a narrowing of the continental shelves, thus allowing more sediment to be dumped beyond the shelf edge, and in turn causing the margins to become unstable. Higher frequencies in the Iberia Abyssal Plain may also be related to earthquake activity in the Eurasian/African plate boundary zone; earthquakes are largely absent from the Madeira Abyssal Plain area and the Canary Basin in general.

The occurrence of earthquakes off the Portuguese margin is well known and associated with the African/Eurasia lithospheric plate

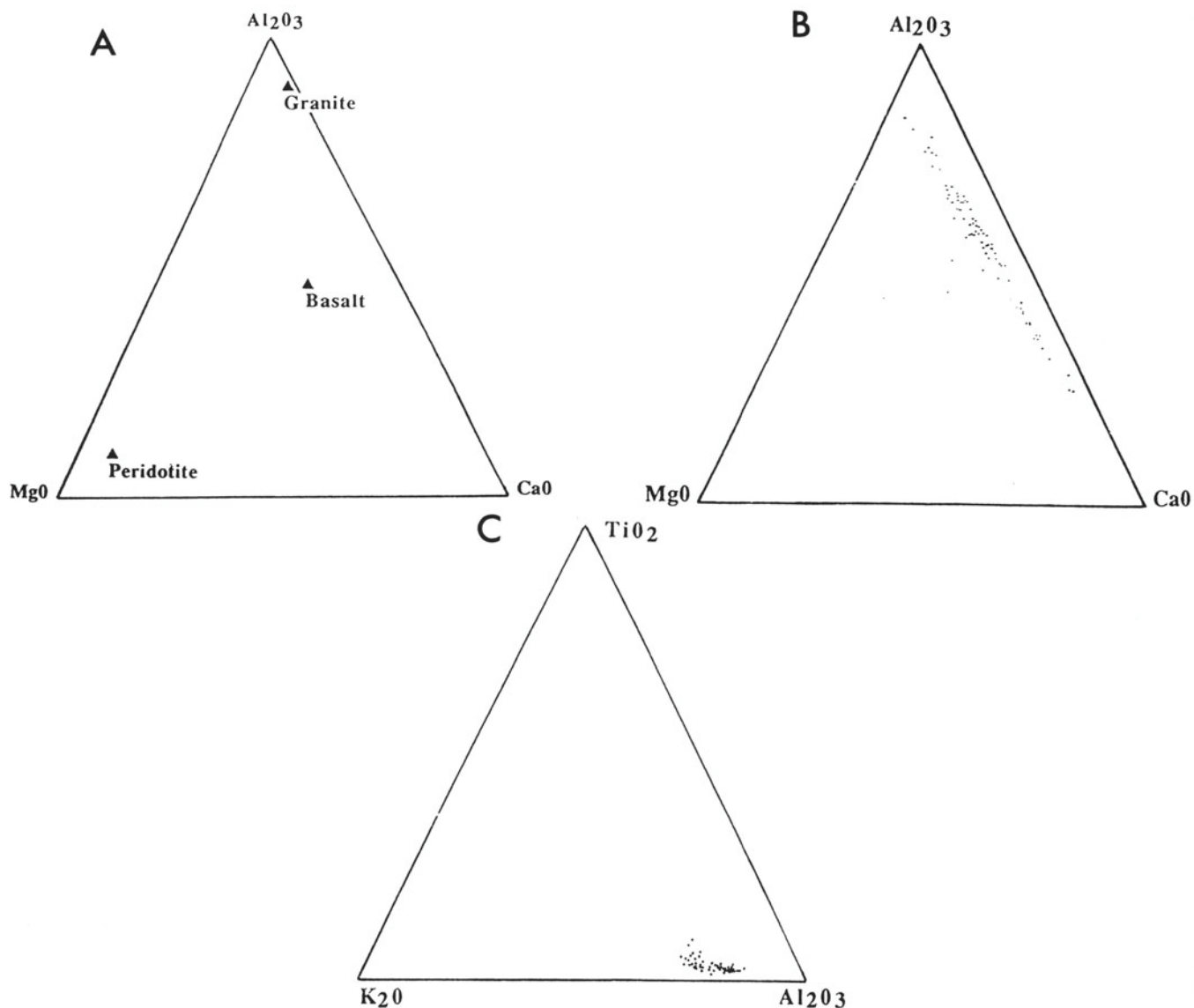


Figure 9. **A.** Expanded triangular diagram of the main composition of possible source rocks (after Matthes, 1983). **B.** Comparison with the distribution of similar elements at Hole 898A showing the broad scatter of values. **C.** Expanded triangular diagram of TiO_2 - K_2O - Al_2O_3 contents indicates the continental source region for Site 898 turbidites.

boundary, which lies to the south of the Iberia Abyssal Plain (Martins and Victor, 1990; Fonseca and Long, 1989). The historic records show several major earthquakes (Moreira, 1985). The most important historical earthquake was the 1755 Lisbon earthquake, with its epicenter located at the Goringe Bank, approximately 300 km south-southwest of Lisbon. There have been ample numbers of earthquakes in the area to generate sediment failures resulting in turbidity currents. However, these earthquakes must also have occurred before the inception of turbidite sedimentation, because we have strong evidence of middle Miocene activity. This took the form of crustal deformation accompanied by a phase of compression in the Rif-Betic Mountains and led to the gentle folding of sediments in the Iberia and northern Tagus Abyssal Plain as seen in seismic reflection profiles (Masson et al., 1994; Mauffret et al., 1989). This compressional phase is probably responsible for the middle to late Miocene hiatus seen at Sites 897 and 898.

The question therefore arises as to why there were no turbidites prior to 2.6 Ma (except for the thin ones in the upper Miocene at Site 900). We postulate that the lowering of sea level that accompanied

the onset of Northern Hemisphere glaciation at 2.6 Ma must have reduced the width of the continental shelves and thus allowed more sediment to be carried over the shelf edge to be deposited on the upper continental slope. Higher rates of accumulation on the upper parts of the slope may have led to unstable sediment accumulation, which could have resulted in earthquake-triggered sediment removal by turbidity flow.

CONCLUSIONS

1. The Pliocene/Pleistocene turbidite sequence comprises muddy turbidites, with sporadic silty and sandy bases, separated by thin layers of pelagic oozes, marls, or clays. The turbidites are usually much less than 1 m thick.
2. Four different types of turbidites can be determined based on color, carbonate, and organic carbon variations: (1) gray terrigenous/siliceous turbidites with mica-rich bases; (2) gray/calcareous terrigenous turbidites with sandy, silty bases; (3)

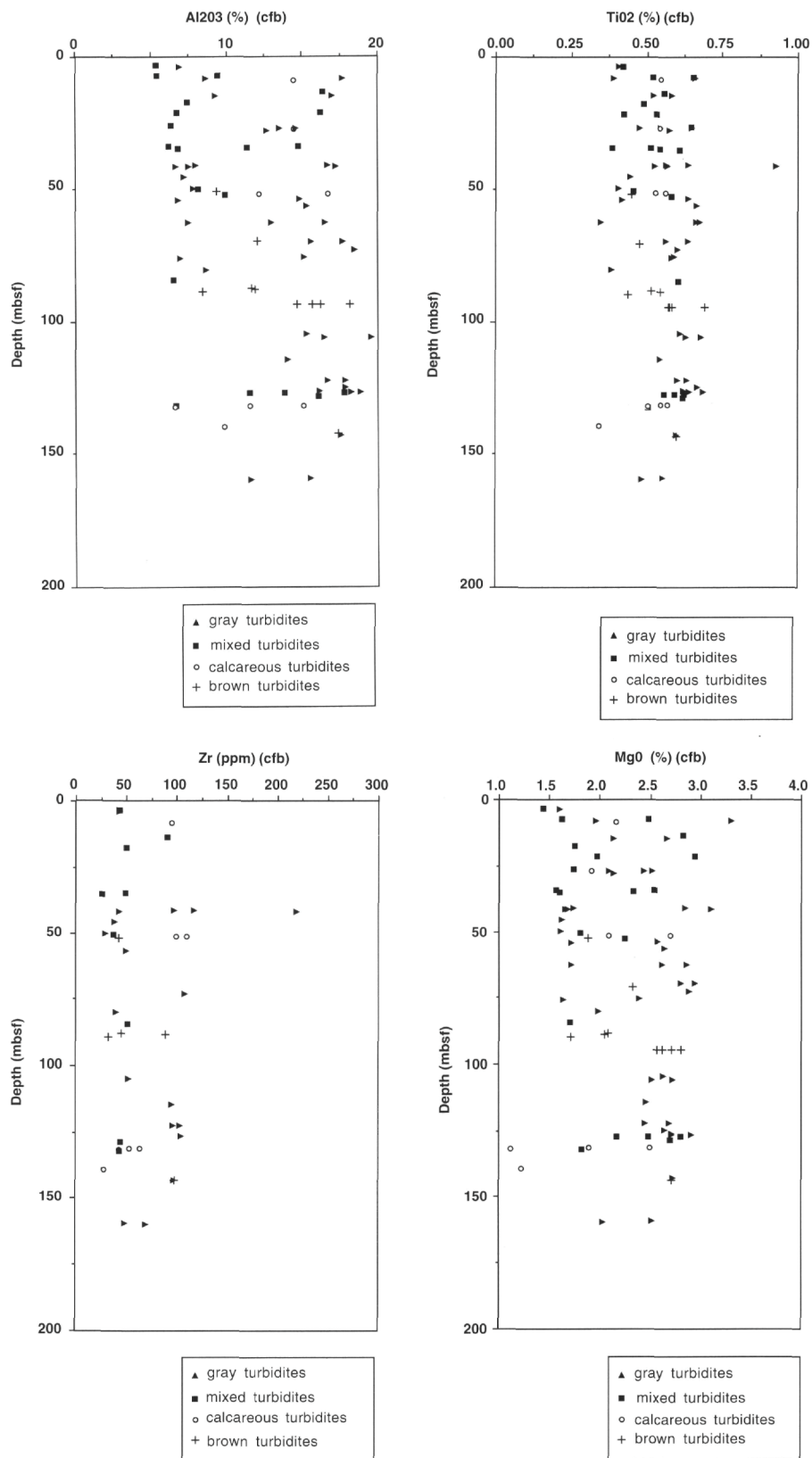


Figure 10. Geochemical profiles of Al₂O₃, TiO₂, Zr, and MgO at Site 898 for the different types of turbidites. All data are plotted on carbonate-free basis.

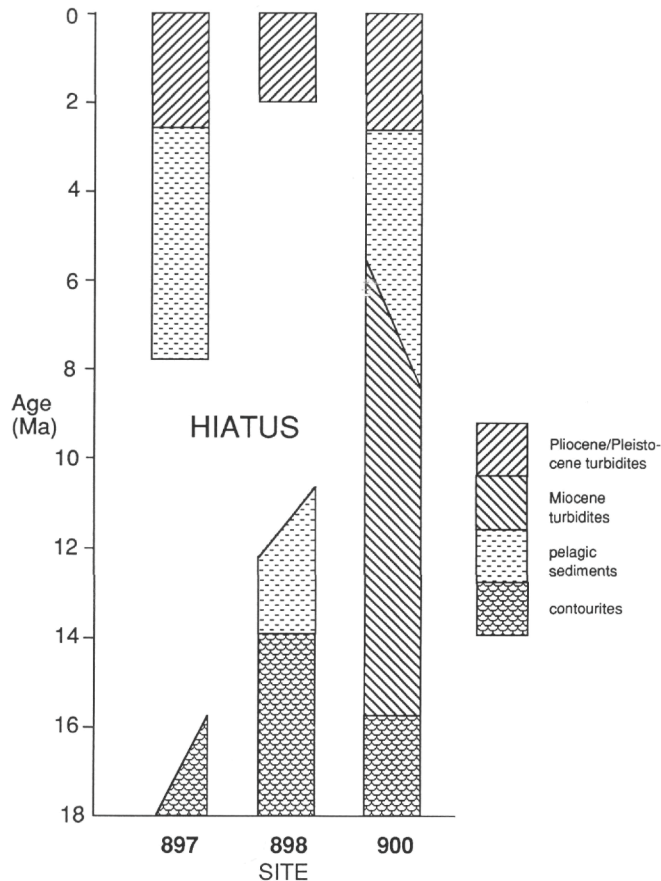


Figure 11. Summary of late Miocene to Pleistocene sedimentation at Sites 897, 898, and 900.

calcareous turbidites with foraminifer-rich bases; and (4) brownish-reddish sandy turbidites common in the lower Pleistocene at all sites. Despite these visual differences, geochemical analysis shows a similar composition for all turbidites.

- Correlation of single turbidites between the drill sites is not possible because of the huge number of small-scale turbidites.
- Major input of terrigenous turbidites into the Iberia Abyssal Plain started in the late Pliocene at 2.6 Ma and followed a period of pelagic deposition that lasted at least a few million years at Sites 897 and 900. At Site 898, the first turbidites were deposited at 2 Ma following a major hiatus. This hiatus also affected Site 897 and is probably related to the regional unconformity that led to formation of the Rif-Betic mountains in southern Spain.
- The frequency of the turbidity currents varies from 20.5 flows/100 k.y. between 1.8 and 2 Ma to 64 flows/100 k.y. between 1.2 to 1.4 Ma, then reduces gradually to the present day. The highest rate of 8 flows/100 k.y. between 1.6 and 2 Ma is at continental rise Site 900. The mechanism for initiating flows appears to be earthquakes, although the onset of Pliocene/Pleistocene turbidite deposition correlates with the onset of Northern Hemisphere glaciation.

ACKNOWLEDGMENTS

D. Milkert would like to thank the Ocean Drilling Program for inviting her to participate in ODP Leg 149. Charlotte Gravestock and Alan Lucas (IOSDL) are thanked for preparing and measuring the carbonate samples. We are grateful to Nigel Higgs and John Thorn-

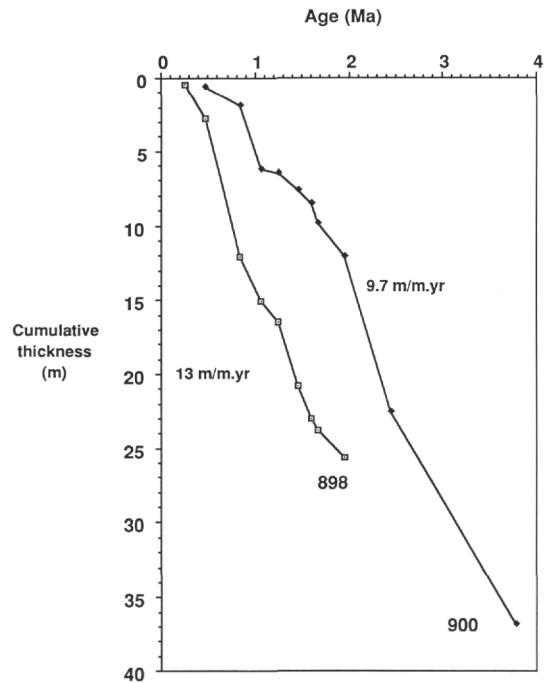


Figure 12. Cumulative thickness of pelagic sediment accumulation through time at Sites 898 and 900. The average accumulation rate at Site 898 is 13 m/m.y., and at Site 900 the accumulation of pelagic sediment averaged 9.7 m/m.y.

son (IOSDL) for the ICP-AES data and helpful discussions on interpretation. We would also like to thank the Shipboard Scientific Party, the ODP technicians, and the SEDCO drilling crew of Leg 149. This manuscript has benefitted from the careful review and helpful comments of Helen Alonso, Antoon Kuijpers, and Doug Masson.

Financial support was provided by NERC (Natural Environment Research Council), United Kingdom (Grant No. GST/02/725), and the EC MAST programme (Grant No. MAS2-CT94-0083).

REFERENCES

- Berger, W.H., 1968. Planktonic foraminifera: selective solution and paleoclimatic interpretation. *Deep-Sea Res. Part A*, 15:31-43.
- Beslier, M.-O., Ask, M., and Boillot, G., 1993. Ocean-continent boundary in the Iberia Abyssal Plain from multichannel seismic data. *Tectonophysics*, 218:383-393.
- Boillot, G., Winterer, E.L., Meyer, A.W., et al., 1987. *Proc. ODP, Init. Repts.*, 103: College Station, TX (Ocean Drilling Program).
- Bouma, A.H., 1962. *Sedimentology of Some Flysch Deposits: A Graphic Approach to Facies Interpretation*. Amsterdam (Elsevier).
- Comas, M.C., and Maldonado, A., 1988. Late Cenozoic sedimentary facies and processes in the Iberian Abyssal Plain, Site 637, ODP Leg 103. In Boillot, G., Winterer, E.L., et al., *Proc. ODP, Sci. Results*, 103: College Station, TX (Ocean Drilling Program), 635-655.
- Crowley, T.J., 1983. Calcium carbonate preservation patterns in the central North Atlantic during the last 150,000 years. *Mar. Geol.*, 51:1-41.
- Davies, T.A., 1967. Recent sedimentation in the Northeast Atlantic [Ph.D. dissert.]. Univ. of Cambridge, U.K.
- de Lange, G.J., Jarvis, I., and Kuijpers, A., 1987. Geochemical characteristics and provenance of late Quaternary sediments from the Madeira Abyssal Plain, North Atlantic. In Weaver, P.P.E., and Thomson, J. (Eds.), *Geology and Geochemistry of Abyssal Plains*. Geol. Soc. Spec. Publ. London, 31:147-165.
- Folk, R.L., 1980. *Petrology of Sedimentary Rocks*. Austin, TX (Hemphill Publ.).
- Fonseca, J.F.B.D., and Long, R.E., 1989. Seismotectonics of Western Portugal. *Proc. 4th Symp. Analysis of Seismicity and Seismic Risk*, Bechyne Castle, Czechoslovakia, 266-273.

Jarvis, I., and Higgs, N., 1987. Trace-element mobility during early diagenesis in distal turbidites: late Quaternary of the Madeira Abyssal Plain, N Atlantic. In Weaver, P.P.E., and Thomson J. (Eds.), *Geology and Geochemistry of Abyssal Plains*. Geol. Soc. Spec. Publ. London, 31:179-214.

Jarvis, I., Pearce, T.J., and Higgs, N.C., 1988. Early diagenetic geochemical trends in Quaternary distal turbidites. *Chem. Geol.*, 95:1-33.

Martins, I., and Victor, L.A.M., 1990. *Contribuicao para o estudo da sismicidade de Portugal continental*. Univ. de Lisboa, Inst. Geofisico do Infante d. Luis, Publ. 18.

Masson, D.G., Cartwright, J.A., Pinheiro, L.M., Whitmarsh, R.B., Beslier, M.-O., and Roeser, H., 1994. Localized deformation at the ocean-continent transition in the NE Atlantic. *J. Geol. Soc. London*, 151:603-613.

Matthes, S., 1983. *Mineralogie*: Berlin (Springer Verlag).

Mauffret, A., Mougnot, D., Miles, P.R., and Malod, J.A., 1989. Cenozoic deformation and Mesozoic abandoned spreading centre in the Tagus abyssal plain (west of Portugal): results of a multichannel seismic survey. *Can. J. Earth Sci.*, 26:1101-1123.

Moreira, V.S., 1985. Seismotectonics of Portugal and its adjacent area in the Atlantic. *Tectonophysics*, 117:85-96.

Pearce, T.J., and Jarvis, I., in press. High resolution chemostratigraphy of Quaternary distal turbidites: a case study of new methods for the analysis and correlation of barren sequences. In Dunay, R.E., and Hailwood, E. A. (Eds.), *Dating and Correlating Biostratigraphically Barren Strata*. Geol. Soc. Spec. Publ. London.

Raymo, M.E., Ruddiman, W.F., and Clement, B.M., 1987. Pliocene-Pleistocene paleoceanography of the North Atlantic at DSDP Site 609. In Ruddiman, W.F., Kidd, R.B., Thomas, E., et al., *Init. Repts. DSDP*, 94 (Pt. 2): Washington (U.S. Govt. Printing Office), 895-901.

Sawyer, D.S., Whitmarsh, R.B., Klaus, A., et al., 1994. *Proc. ODP, Init. Repts.*, 149: College Station, TX (Ocean Drilling Program).

Shackleton, N.J., Backman, J., Zimmerman, H., Kent, D.V., Hall, M.A., Roberts, D.G., Schnitker, D., Baldauf, J.G., Desprairies, A., Homrighausen, R., Huddleston, P., Keene, J.B., Kaltenback, A.J., Krumsiek, K.A.O., Morton, A.C., Murray, J.W., and Westberg-Smith, J., 1984. Oxygen isotope calibration of the onset of ice-rafting and history of glaciation in the North Atlantic region. *Nature*, 307:620-623.

Shackleton, N.J., Crowhurst, S., Hagelberg, T., Pisias, N.G., and Schneider, D.A., 1995. A new late Neogene time scale: application to Leg 138 sites. In Pisias, N.G., Mayer, L.A., Janecek, T.R., Palmer-Julson, A., and van Andel, T.H. (Eds.), *Proc. ODP, Sci. Results*, 138: College Station, TX (Ocean Drilling Program), 73-101.

Stow, D.A.V., and Piper, D.J.W., 1984. Deep-water fine-grained sediments: history methodology and terminology. In Stow, D.A.V., and Piper, D.J.W. (Eds.), *Fine-Grained Sediments: Deep-Water Processes and Facies*. Geol. Soc. Spec. Publ. London, 15:3-14.

Totland, M., Jarvis, I., and Jarvis, K.E., 1992. An assessment of dissolution techniques for the analysis of geological samples by plasma spectrometry. *Chem. Geol.*, 95:35-62.

Weaver, P.P.E., and Kuijpers, A., 1983. Climatic control of turbidite deposition on the Madeira Abyssal Plain. *Nature*, 306:360-363.

Weaver, P.P.E., Searle, R.C., and Kuijpers, A., 1986. Turbidite deposition and the origin of the Madeira Abyssal Plain. In Summerhayes, C.P., and Shackleton, N.J. (Eds.), *North Atlantic Palaeoceanography*. Spec. Publ. Geol. Soc. London, 21:131-143.

Weaver, P.P.E., Thomson, J., and Hunter, P., 1987. Introduction. In Weaver, P.P.E., and Thomson, J. (Eds.), *Geology and Geochemistry of Abyssal Plains*. Geol. Soc. Spec. Publ. London, 31:vii-xii.

Wentworth, C.K., 1922. A scale of grade and class terms of clastic sediments. *J. Geol.*, 30:377-392.

Date of initial receipt: 5 December 1994

Date of acceptance: 10 July 1995

149SR-203

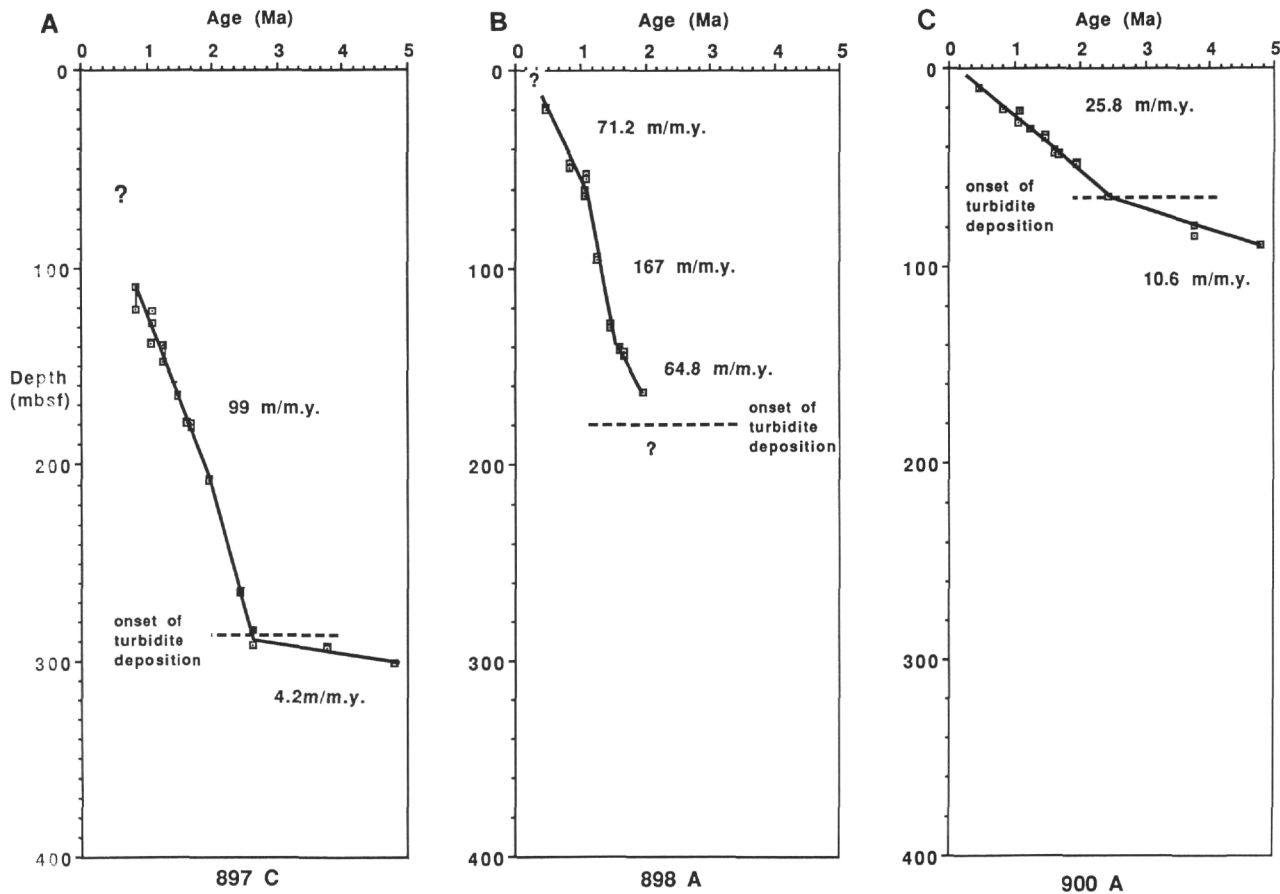


Figure 13. Age vs. depth plots for Holes 897C, 898A, and 900A show the variation in the rate of total sediment accumulation through time and across the margin.

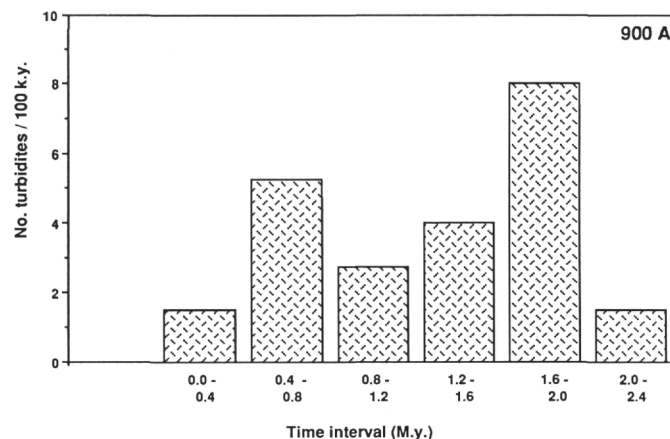
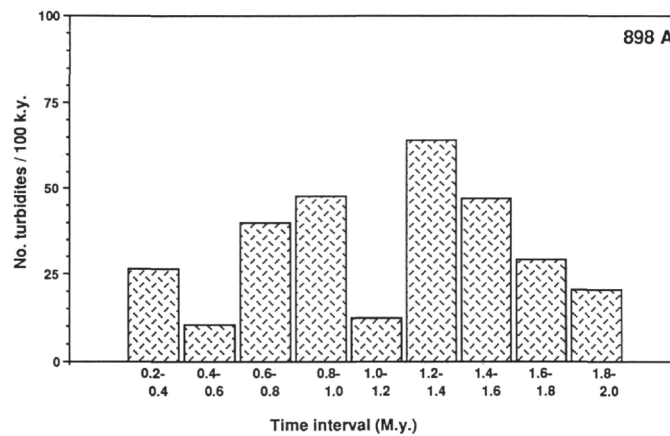


Figure 14. Accumulation of turbidites over 200,000 yr at Hole 898A; accumulation of turbidites over 400,000 yr at Hole 900A.